PCCP

PAPER

View Article Online
View Journal

Cite this: DOI: 10.1039/c8cp07332e

Dissociative photoionization of CF_3Cl *via* the C^2E and D^2E states: competition of the C–F and C–Cl bond cleavages

Xiangkun Wu,[a] Tongpo Yu,[a] Yan Chen,[b] Xiaoguo Zhou, *[a] Shilin Liu,[a] Xinhua Dai,[b] Fuyi Liu[c] and Liusi Sheng[c]

The dissociative photoionization of CF_3Cl was investigated using threshold photoelectron photoion coincidence (TPEPICO) imaging in the energy range of 12.30–18.50 eV. The coincident time-of-flight mass spectra and three-dimensional time-sliced images of the CF_2Cl^+ fragment were recorded at a few specific photon energies. Two fragmentation pathways were observed that led to the breakage of the C–Cl and C–F bonds, while the branching ratio elicited an energy-dependent relationship. The CF_3^+ fragment was dominant in the dissociation of the X^2E, A^2A' and B^2A'' states, while CF_2Cl^+ became the predominant fragment and its branching ratio remained constant in the energy range associated with the C^2E and D^2E states. Based on the inflection point in the energy-dependent curve of the fragment branching ratios, the adiabatic ionization energy (IE_a) of C^2E is suggested to be 15.46 eV. Although the excess energy increased considerably from C^2E to D^2E, the kinetic energy release distributions (KERDs) of CF_2Cl^+ were similar. Moreover, the anisotropy parameters β for the F-loss channel were positive and larger than those for the Cl-loss channel. The calculated F-loss potential energy curves of CF_3Cl^+ suggested that for the C^2E and D^2E states, the C–F bond rupture occurred *via* the internal conversion to the A^2A' state followed by the dissociation attributed to the crossing of the barrier along the C–F coordinate. Based on the experimental and theoretical conclusions, the internal conversion is the rate-determining step in the dissociative photoionization of CF_3Cl *via* the C^2E and D^2E ionic states, irrespective of whether the C–F and C–Cl bonds rupture.

Received 29th November 2018,
Accepted 1st February 2019

DOI: 10.1039/c8cp07332e

rsc.li/pccp

1. Introduction

Chlorofluorocarbons have been extensively investigated because they are very useful in industrial applications, *e.g.*, plasma etching of silicon wafer semi-conductor devices,[1,2] and highly reactive plasma reactions.[3] However, the halogen atoms produced in the dissociation of chlorofluorocarbons by the solar ultra-violet (UV) light in the atmosphere are believed to play a significant role in the catalytic depletion of the stratospheric ozone.[4,5] Therefore, the UV photodissociation of chlorofluorocarbons has attracted considerable attention. Similar to the dissociation of neutral chlorofluorocarbons, dissociative photoionization of CF_3Cl also produces F and Cl atoms simultaneously by breaking the C–F and C–Cl bonds by the action of VUV photons. However, the contribution of CF_3Cl^+ has been ignored with the lack of information on dissociation dynamics of the latter. Compared to chloride atoms, fluoride atoms are relatively harmless to ozone. Thus, the competition of the C–Cl and C–F bond cleavages of the CF_3Cl^+ ion is an interesting topic relevant to the reduction of the quantum yield of chloride atoms, for the in-depth understanding of the corresponding dissociation mechanisms and dynamics.

The neutral CF_3Cl molecule has C_{3v} symmetry, and its valence-shell electron configuration in the ground state is $[core](4a_1)^2(3e)^4(4e)^4(1a_2)^2(5a_1)^2(5e)^4$. The outer (5e) orbitals consist of the lone pairs of the chlorine atom, the $(5a_1)$ orbital corresponds to the σ(C–Cl) bond, and the $(1a_2)$, (4e), and (3e) electrons are essentially associated with the lone pairs of three fluorine atoms.[6–8] The X^2E, A^2A_1, B^2A_2, C^2E and D^2E ionic states can be prepared by removing an electron from these molecular orbitals, (5e), $(5a_1)$, $(1a_2)$, (4e) and (3e), respectively.

Molecular spectroscopy of the CF_3Cl^+ ion in low-lying electronic states was extensively studied by many experimental approaches, *e.g.* absorption spectroscopy,[9,10] electron energy loss spectroscopy,[11–13] penning ionization electron spectroscopy,[14] vacuum-UV

[a] *Hefei National Laboratory for Physical Sciences at the Microscale, iChEM (Collaborative Innovation Center of Chemistry for Energy Materials), Department of Chemical Physics, University of Science and Technology of China, Hefei 230026, China. E-mail: xzhou@ustc.edu.cn*
[b] *National Institute of Metrology, Beijing 100013, China*
[c] *National Synchrotron Radiation Laboratory, University of Science and Technology of China, Hefei 230029, China*

(VUV) fluorescence spectroscopy,[15–17] photoelectron spectroscopy (PES),[6–8,18–24] and threshold photoelectron spectroscopy (TPES).[10,25,26] In these spectroscopies, no vibrational structure was resolved in X^2E, A^2A_1, B^2A_2, and C^2E states. An inconsistent conclusion for the D^2E state that only a few vibrational peaks were observed in the He I and He II PES,[6–8] but they disappeared in TPES.[10,25,26] From these measurements, the adiabatic and vertical ionization energies of the CF_3Cl molecule were derived to be 12.46 and 13.10 eV, respectively, and the vertical ionization energies of the A^2A_1, B^2A_2, C^2E, and D^2E states were 15.0, 15.5, 16.5 and 17.4 eV, respectively.[8–10,23]

Once the internal energy exceeds the dissociation limits, the C–Cl and C–F bond cleavages of CF_3Cl^+ may occur to produce the fragment ion of CF_3^+ and CF_2Cl^+, respectively. Electron impact ionization,[11,27] photoionization mass spectrometry,[10,28,29] and threshold photoelectron photoion coincidence (TPEPICO) spectroscopy[26] were applied to investigate the dissociation dynamics of the CF_3Cl^+ cation. The appearance potentials (AP_0) of various fragments were reported as $AP(CF_3^+/CF_3Cl) = 12.79$ eV[26] and $AP(CF_2Cl^+/CF_3Cl) = 14.30$ eV.[25] The dynamics of the Cl-loss pathway in the low-lying electronic states was investigated using photoelectron photoion coincidence (PEPICO) spectroscopy[30,31] and threshold photoelectron photoion coincidence spectroscopy.[25,26] The kinetic energy release distribution (KERD) and angular distribution of CF_3^+ were measured, and the C–Cl bond breaking from the X^2E state progressed statistically. For the excited electronic states of CF_3Cl^+, *e.g.* A^2A_1/B^2A_2, C^2E, and D^2E, the KERDs of CF_3^+ exhibited a bimodal distribution, whereby a faster, parallel dissociation was dominant together with a statistical distribution.[26]

Compared to the Cl-loss channel, the $CF_2Cl^+ + F$ dissociation pathway of CF_3Cl^+ is rarely mentioned in the reported literature. Although the $AP_0(CF_2Cl^+/CF_3Cl)$ value was lower than the A^2A_1/B^2A_2 energies, the CF_2Cl^+ fragments were mainly observed in the dissociation of the C^2E and D^2E states. Through fitting the time-of-flight profile of the CF_2Cl^+ ion, the total KERD was roughly obtained for the dissociation of CF_3Cl^+ in the C^2E and D^2E states.[25,31] For the F-loss process of the C^2E state, the KERD of the CF_2Cl^+ fragment fitted very well with an impulsive model of early dissociation, while, the average released kinetic energy of CF_2Cl^+ dissociated from $CF_3Cl^+(D^2E)$ was less than the predicted result of the classical impulsive model, but substantially larger than that predicted by the phase-space theory. Moreover, the energy release was completely independent of the vibrational excitation. Thus, Powis[31] and Creasey *et al.*[25] suggested that the F-losses from both the C^2E and D^2E states were non-statistical and resembled a direct dissociation. However, as suggested in our recent dynamic investigation of the Cl-loss process for CF_3Cl^+,[26] the C–Cl bond cleavages of the C^2E and D^2E states should be relatively slow as the internal conversion to the repulsive A^2A_1 state must occur to produce the CF_3^+ fragment. This indicates that both the C^2E and D^2E states are adiabatically bound whatever along the C–Cl and C–F bond ruptures. In addition, the KERDs obtained previously[25,31] by fitting the CF_2Cl^+ TOF profile with an approximation of a single isotopic Cl (a mass of 35.5 u) were a bit cursory. Therefore, the C–F bond breaking mechanisms of the C^2E and D^2E states must be rechecked. A more accurate KERD and a detailed angular distribution of the CF_2Cl^+ fragment are necessary in association with the high-level potential energy surfaces, to infer the corresponding dissociation mechanism.

As described previously, TPEPICO imaging is a powerful experimental approach used to investigate the dissociation dynamics of the internal energy-selected cations.[32–34] Specifically, a more accurate KERD and a detailed angular distribution of the specific fragment ion can be measured simultaneously, compared to the traditional method of fitting the TOF profile.[35–39] Herein, the dissociative photoionization of the CF_3Cl molecule *via* the C^2E and D^2E ionic states has been re-investigated. Moreover, the F-loss potential energy curves of CF_3Cl^+ in the low-lying electronic states are calculated using density functional theory. Combining the experimental and theoretical results, CF_2Cl^+ and F fragmentation mechanisms of the CF_3Cl^+ ion in the C^2E and D^2E states are proposed, and the competition between the C–Cl and C–F bond cleavages is fully discussed.

2. Experimental and computational

The present experiment was performed at the U14-A beamline of the National Synchrotron Radiation Laboratory, Hefei, China. The details of the beamline and the TPEPICO velocity map imaging spectrometer have been described previously,[32,40] and only a brief introduction is outlined herein. The VUV photons of synchrotron radiation were produced from an undulator and dispersed using a 6 m monochromator with an energy-resolving power ($E/\Delta E$) of $\sim$2000 at 15 eV. The higher-order harmonic radiation was suppressed using a rare gas filter filled with neon. The absolute energy of the VUV photons was calibrated in TPES with the use of the well-known ionization energies of argon and neon, and the photon flux was measured with a silicon photodiode.

The commercial CF_3Cl gas (a purity of 99.9%) with a stagnation pressure of 1.0×10^5 Pa was injected into a vacuum chamber through a 30 μm-diameter nozzle. The continuous supersonic molecular beam was collimated using a 0.5 mm-diameter skimmer and was then perpendicularly intersected with the VUV light at 10 cm downstream from the nozzle. The electrons and ions produced in the dissociative photoionization process were extracted and accelerated in opposite directions by a direct current extraction field ($\sim$15 V cm^{-1}). The double velocity map imaging method was used to collect both threshold electrons and ions simultaneously. Through the use of the decelerated electric field[41] and the subtraction method,[42] the contamination of hot electrons in TPES was efficiently suppressed. The TPEPICO TOF mass spectra were measured using a single-start multiple-stop data acquisition mode, in which the threshold photoelectrons were used as the start signals.[43] The coincident ions were directly projected on two 40 mm-diameter multichannel plates backed by a phosphor screen (Burle Industries, P20), and the corresponding velocity map images were recorded using a thermoelectric-cooling CCD camera (Andor, DU934N-BV). When the image of a specific ion was acquired, a high-voltage pulse

(DEI, PVM-4210) was applied at the MCPs of the ion detector as a mass gate. The minimum effective duration time of the mass gate was ~40 ns to obtain the time-sliced images.

The quantum chemical calculations were performed using the Gaussian 09W program package (D.01 version 9.5).[44] The optimized geometries and energies of the neutral CF_3Cl molecule and its cation in the ground state were calculated at the B3LYP/6-311+G(d) level of theory. The potential energy surfaces of several low-lying electronic states of CF_3Cl^+ were calculated by using a time-dependent density functional theory (TD-DFT) method with a 6-311+G(d) basis set. A partial optimization method was used to describe the F-loss and Cl-loss potential energy curves of the lowest eight electronic states, as described in our recent calculations.[26] At every given C–F or C–Cl distance, the other geometrical parameters were re-optimized. The electronic configuration of each ionic electronic state was carefully checked to confirm its symmetry in the open-shell excited species.

3. Results and discussion

3.1 TPEPICO time-of-flight mass spectra

The threshold photoelectron spectrum of CF_3Cl in the photon energy range of 12.30–18.30 eV was recorded, which was shown in a previous paper.[26] The five low-lying electronic states of CF_3Cl^+, *e.g.*, X^2E, A^2A_1, B^2A_2, C^2E and D^2E ionic states are involved in the energy range. To investigate the fragmentation of the CF_3Cl^+ ion in specific states, the TPEPICO mass spectra were recorded at various photon energies. Both the Cl-loss and F-loss fragmentation pathways were observed. Thus, to facilitate a comparison of the different dissociation channels, Fig. 1 displays the mass spectra at several typical energies, *e.g.* 12.75 eV for X^2E, 14.88 eV for A^2A_1, 15.36 eV for B^2A_2, 15.83, 16.13, 16.48 and 16.99 eV for C^2E, and 17.85 eV for the D^2E state. In the X^2E state, the parent ion, CF_3Cl^+ (*m*/*z* 104, 106), can be observed, and the unique fragment of CF_3^+ (*m*/*z* 69) also appears. In the A^2A_1 and B^2A_2 states, the CF_3^+ ions dominate but the CF_2Cl^+ (*m*/*z* 85 or 87) fragment ion appears to have a very limited fraction. Interestingly, the TOF profiles of CF_3^+ and CF_2Cl^+ fragments yield different contours: a broadened triangle is superimposed on a terraced background for CF_3^+ (Fig. 3 in ref. 26), while only a triangle-like background for CF_2Cl^+. With the increase in photon energy in the C^2E state, the relative intensity of the CF_2Cl^+ fragment begins to grow rapidly. At an excitation energy of 16.99 eV for the C^2E state and 17.85 eV for the D^2E state, the CF_2Cl^+ intensity is far beyond that for the CF_3^+ fragment, indicating that the C–F bond rupture is the dominant dissociation channel for the C^2E and D^2E states.

As shown in our previous experiment,[26] no CF_3Cl^+ ions existed beyond 12.79 eV in threshold photoionization, thus implying that the parent ions were fully dissociated. Fig. 2 shows the branching ratios of the Cl-loss and F-loss fragmentation of the CF_3Cl^+ ion at various photon energies. Apparently, the variations of the branching ratios yield near-sigmoid functional curves. Below 15.2 eV, the relative abundance of CF_3^+ is constant and equals to 95%. The relative abundance of CF_2Cl^+ rapidly increased for energies ≥15.2 eV, and almost equals that of CF_3^+ at 16.13 eV. Finally, the CF_2Cl^+ abundance is increased to 0.71 and is kept constant for the C^2E and D^2E states. As proposed previously,[26] the Cl-loss of CF_3Cl^+ for both the C^2E and D^2E states occurred *via* the internal conversion to the repulsive A^2A_1 state followed by dissociation. Similar dissociation mechanisms are expected for the C–F bond rupture of CF_3Cl^+ in the C^2E and D^2E states, as described in detail in Section 3.5. Thus, the sudden change in the branching ratios in Fig. 2 should respond to the appearance of the C^2E state. Therefore, the adiabatic ionization energy (IE_a) of C^2E is approximately determined to be 15.46 eV at the cross point of the lag and growth phases (Fig. 2). This value is also exactly located at the starting point of the C^2E state in TPES of Fig. 1. In addition, the close branching ratios of the two dissociation pathways for the C^2E and D^2E states imply that the low-energy electronic states in which internal conversion occurs may be the same.

It is worth noting in Fig. 1 that for the C^2E and D^2E states, the TOF profiles of CF_2Cl^+ become an approximate trapezoid, while those of CF_3^+ form a broad triangle. Actually, as indicated previously,[36,39] the trapezoid-like profile usually correlates with the convolution between a non-statistical KERD from a parallel dissociation and a Gaussian-type instrument response function,

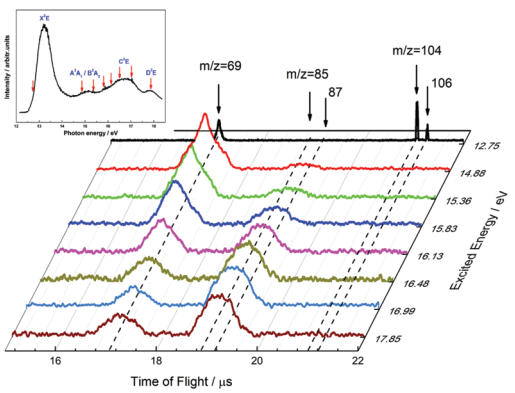

Fig. 1 TPEPICO time-of-flight mass spectra of the dissociative photoionization of CF_3Cl at various photon energies, where the threshold photoelectron spectrum is shown in the inserted panel.

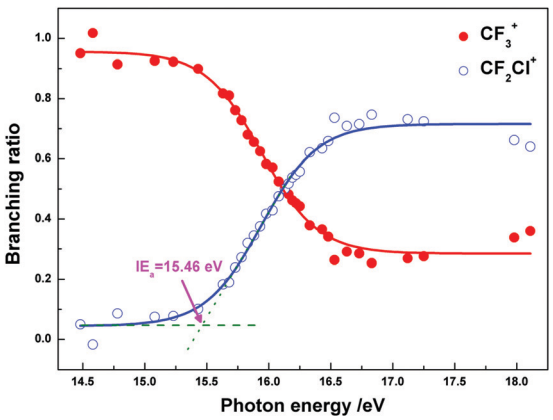

Fig. 2 Branching ratios of Cl- and F-loss pathways of CF_3Cl^+ at various photon energies.

while the triangle is attributed to a statistical distribution. Therefore, different dissociation mechanisms are expected for CF_3^+ and CF_2Cl^+ fragments in C^2E/D^2E electronically excited states. Moreover, the full widths of the CF_3^+ and CF_2Cl^+ peaks are expanded and have values higher than 1 μs for all the electronic excited states, thus implying that a part of excess energy is released into a translational degree of freedom of fragments during the dissociation process.

As mentioned above, the contradictory conclusions have been drawn based on the previous[25,31] and recent[26] experiments for the lifetimes of the C^2E and D^2E states. Based on the analysis of the TOF profiles of the fragment ions, the findings from previous experiments[25,31] claim that C^2E is a direct and fast dissociative state according to C–Cl bond breakage. However, the TOF profile of the fragment ion can change with the polarization of the photon. Usually, the kinetic energy distribution is reliably derived from the TOF fitting when the photon polarization is kept at the magic angle. Unfortunately, it is almost impossible to change the polarization of the VUV photons from the synchrotron radiation and He I light. As indicated by the recent calculation,[26] the C^2E state was typically bound along the C–Cl coordinate, and CF_3^+ fragments must therefore be produced *via* internal conversion from C^2E to the lower repulsive electronic states.

To our surprise, the TOF width of the CF_2Cl^+ fragment dissociated from CF_3Cl^+ in A^2A_1/B^2A_2, C^2E and D^2E states is kept near constant, although the excess energy along the pathway, $CF_3Cl^+ \rightarrow CF_2Cl^+(X^1A') + F(^2P)$, is dramatically increased from the A^2A_1/B^2A_2 to the C^2E and D^2E states. Therefore, a complicated dissociation mechanism is expected for the F-loss of CF_3Cl^+ in the electronic excited states, in which the partially available energy may be released prior to the dissociation. In fact, similar phenomena have also been observed in the C–Cl bond rupture of the C^2E and D^2E states.[26] Owing to too weak intensity and a small branching ratio, the F-loss channel of CF_3Cl^+ in the A^2A_1 and B^2A_2 states is neglected in the following discussion. Accordingly, attention is only paid to the C–F bond cleavage mechanism of the C^2E and D^2E ionic states.

3.2 Kinetic energy distribution of CF_2Cl^+ dissociated from C^2E and D^2E states

To obtain more details on the translation energy and angular distributions, the velocity map images of the CF_2Cl^+ fragments were recorded for CF_3Cl^+ in the C^2E and D^2E states. Since there are two isotopes of the Cl atom, the CF_2Cl^+ peak in Fig. 1 actually must be the sum of the two TOF peaks, $CF_2{}^{35}Cl^+$ and $CF_2{}^{37}Cl^+$, with their natural abundance. Therefore, deconvolution of the trapezoid-like TOF peak is necessary to get the individual contribution of a single isotope like $CF_2{}^{35}Cl^+$. Fig. 3 shows the experimental and fitted coincident TOF profile of CF_2Cl^+ recorded at 17.85 eV. When the 40 ns mass gate of the detector was applied, only a very small amount (less than 5%) of the other isotope component, $CF_2{}^{37}Cl^+$, was involved and it should have a negligible contribution in the image. A similar result was also obtained for the analyses of the CF_2Cl^+ peak at 16.99 eV, which is not shown yet.

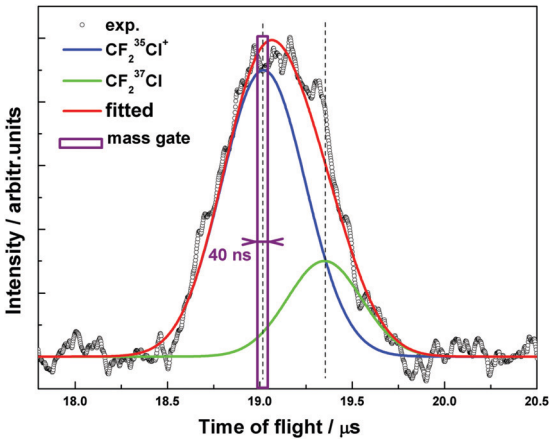

Fig. 3 The experimental and fitted coincident time-of-flight profile of CF_2Cl^+ dissociated from CF_3Cl^+ in the D^2E state at 17.85 eV. The purple square shows the time position of the mass gate.

With an extraction field of 14 V cm^{-1}, the resolving power of the translation energy of the present TPEPICO imaging is better than 3%,[32] and the three-dimensional time-sliced images of the $CF_2{}^{35}Cl^+$ fragment at 16.99 and 17.85 eV are shown in Fig. 4(a and b), respectively.

In the images of Fig. 4, the molecular beam propagates along the horizontal direction and the electric vector ε of the VUV photon is vertical. At 16.99 and 17.85 eV, the two images are similar and comprise of a single wide ring. The anisotropic distributions are observed for both the rings, and the major population is along the polarization direction of the VUV photon. Surprisingly, the diameters of the two rings are almost identical, and only the ring at 17.85 eV looks thicker, although the excitation energies are considerably different. Based on the accumulation of the intensity of the image as a function of angle, the speed distribution of $CF_2{}^{35}Cl^+$ was obtained. Taking into account the conservation of linear momentum, the total KERD was acquired and is shown in Fig. 5(a and b). The results of the Cl-loss pathways in ref. 26 are also shown in Fig. 5 for comparison.

For both the images at 16.99 and 17.85 eV, the corresponding curves for the total KERD of the F-loss pathway can be fitted very well with the Gaussian-type profile, thus indicating that the

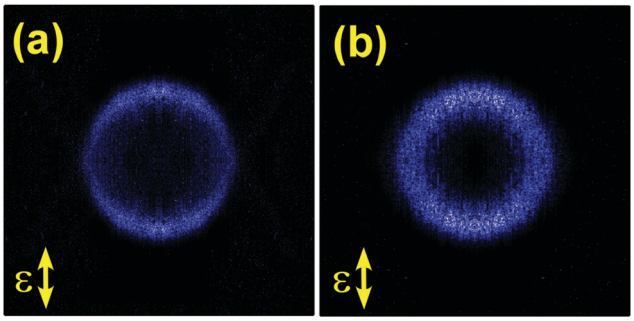

Fig. 4 3D TPEPICO time-sliced velocity map images of $CF_2{}^{35}Cl^+$ and the corresponding total kinetic energy distributions at 16.99 eV (a) and 17.85 eV (b).

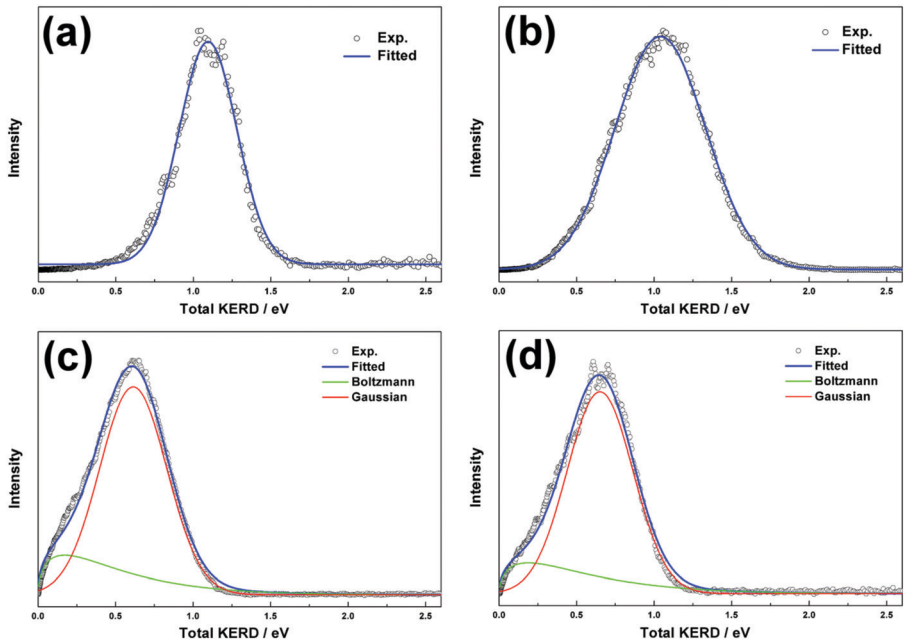

Fig. 5 Total kinetic energy distributions of the F-loss pathway at 16.99 eV (a) and 17.85 eV (b). Corresponding distributions of the Cl-loss channel at 16.99 eV (c) and 17.85 eV (d).

kinetic energy distribution in the F-loss process of the C^2E and D^2E ionic states is non-statistical in nature. In other words, the C–F bond cleavage occurs at a relatively faster rate compared to the full IVR once being excited to the C^2E and D^2E states. An atypical phenomenon is observed that the average total kinetic energy is 1.10 eV at 16.99 eV, but this energy actually decreases to 1.04 eV at 17.85 eV although the excess energy is increased by 0.86 eV, agreeing with the observations of Creasey *et al.*[25] Moreover, more details of KERD are revealed from the images. The maximal released kinetic energies are 1.61 eV at 16.99 eV and 1.84 eV at 17.85 eV.

For the dissociation along a repulsive potential energy surface, the classical "impulsive model" is usually used to estimate the proportion of the average total kinetic energy $\langle E_T \rangle$ and the available energy E_{avail} based on the following eqn (1),

$$f_T = \frac{\langle E_T \rangle}{E_{avail}} = \frac{\mu_{C-F}}{\mu_{CF_2{}^{35}Cl-F}} = 0.474 \quad (1)$$

where μ is the reduced mass.[45] The accurate dissociation limit of $CF_2Cl^+(X^1A') + F(^2P)$ is unknown, so the estimated value, 14.30 eV, from ref. 25 was used to evaluate the excess energy along the dissociation pathway. As shown in Table 1, the f_T value at 16.99 eV is 0.41 and close to the values reported by Powis[31] and Creasey *et al.*[25] Since the CF_2Cl^+ fragment is in a non-planar configuration at the instant of energy release (early energy release), a small part of the excess energy may be bounded to deform the CF_2Cl^+ fragment from the non-planar geometry to the planar structure in the ground state. Thus, a slight difference between the experimental and predicted f_T values can be acceptable.[25,31] At 17.85 eV, the f_T value is only 0.293, which is almost half of the predicted value based on the impulsive model. Thus, partial IVR might occur for the D^2E ionic state prior to dissociation, and most of the excess energy will be redistributed to the other degrees of freedom except the C–F stretching vibration, thus yielding a longer lifetime for D^2E compared to that for the C^2E state.

Table 1 Available energies, average total kinetic energies $\langle E_T \rangle$ and anisotropy parameters β of the $CF_2{}^{35}Cl^+$ fragment dissociated from the $CF_3{}^{35}Cl^+$ ion in the C^2E and D^2E states[a]

$h\nu$/eV	Ionic state	E_{avail}/eV	$\langle E_T \rangle$/eV	f_T	β
16.99	$C^2E(^2A'/^2A'')$	2.69	1.10	0.407	0.73 ± 0.02
17.85	$D^2E(^2A'/^2A'')$	3.55	1.04	0.293	0.35 ± 0.01

[a] The estimated dissociation limit of $CF_2Cl^+(X^1A') + F(^2P)$ is used as 14.30 eV from ref. 25.

3.3 Angular distribution of the $CF_2{}^{35}Cl^+$ fragment ion

The angular distribution of the fragment ion of $CF_2{}^{35}Cl^+$, $I(\theta)$, was obtained by integrating the images in Fig. 4 over an appropriate range of speeds at each angle. The anisotropy parameter β of the specific dissociation pathway can then be derived from fitting $I(\theta)$ with eqn (2),[46]

$$I(\theta) = \frac{1}{4\pi}[1 + \beta \cdot P_2(\cos\theta)] \quad (2)$$

where θ is the angle between the recoil velocity of the fragment and the electric vector ε of the VUV photon, and $P_2(\cos\theta)$ is the second-order Legendre polynomial. If the dissociation that occurs within a certain period is much longer than the molecular rotational period, the β value equals to zero. When the ion lifetime is less than the rotational period, the dissociation is very fast with a β value which is far from zero, *e.g.*, β = 2 for parallel

dissociation, and $\beta = -1$ for the perpendicular decomposition of the diatomic molecule.

As shown in Table 1, the β values of $CF_2{}^{35}Cl^+$ are determined to be 0.73 at 16.99 eV and 0.35 at 17.85 eV. Both the positive values imply that the C–F bond cleavages of the two states have a parallel dissociation tendency, and the dissociation rates are faster than the molecular rotational period. However, taking into account the fact that their values are much smaller than two, the potential energy curves of the C^2E and D^2E states along the C–F distance might not be repulsive in the Franck–Condon region, otherwise the β values should be close to two. A detailed discussion is introduced in the following section with the aid of the calculated potential energy curves of the low-lying electronic states of CF_3Cl^+.

3.4 F-loss potential energy curves of CF_3Cl^+ in low-lying electronic states

It is very difficult to propose a reliable dissociation mechanism for the F-loss of CF_3Cl^+ in the electronic excited states, with the lack of their potential energy surface. Therefore, we calculated the potential energy curves of CF_3Cl^+ in the low-lying electronic states along the C–F bond cleavage based on TD-DFT, similar to our previous work on the Cl-loss potential energy curves.[26] During the F-loss or Cl-loss fragmentation, the initial C_{3v} symmetry of CF_3Cl^+ would be degenerated to the C_s symmetry. Hence, the original ^2E degenerate state would split into A′ and A″ states.

Although it is difficult to accurately calculate the excitation energies at the TD-B3LYP/6-31+G(d) level without involving multi-reference configuration interactions, the major electronic configurations and dissociative features of the low-lying electronic states can be predicted reliably, *e.g.*, $C_2H_3F^{+}$[47] and $C_2H_3Cl^+$.[48] As shown in our previous calculations,[26] the B^2A'', $C(^2A'/^2A'')$ and $D(^2A'/^2A'')$ ionic states of CF_3Cl^+ were bound along the C–Cl bond, while the $A^2A'(A^2A_1)$ state was repulsive in the Franck–Condon region owing to the removal of an electron from the σ(C–Cl) bond. Therefore, the partial optimization method was performed to calculate the C–F bond rupture potential energy curves of the $X(^2A'/^2A'')$, B^2A'', $C(^2A'/^2A'')$ and $D(^2A'/^2A'')$ bound states, but we failed to apply it in the A^2A' state because no local minimum could be found on such a repulsive potential energy surface. In this case, to calculate the C–F cleavage potential energy curve of A^2A', a C–Cl distance was fixed to be 1.773 Å as the optimized length in the neutral CF_3Cl molecule during the optimization of the A^2A' ionic state along the C–F bond length. Similarly, that with a larger C–Cl distance of 2.0 Å was also calculated for comparison. Based on this hypothesis, the interaction among A^2A' and the higher electronic states could be estimated, and the dissociative characteristics of the A^2A' ionic state along the C–F bond could be qualitatively obtained.

Fig. 6 displays the calculated F-loss potential energy curves of the CF_3Cl^+ ion in various electronic states. Only the $X(^2A'/^2A')$ and A^2A' ionic states adiabatically correlate with the lowest C–F rupture channel of $CF_2Cl^+(X^1A') + F(^2P)$, while the other electronic states adiabatically link to the higher energy channels (beyond the present excitation energy range). The ground $X(^2A'/^2A')$ state is stable, but the A^2A' state shows the predissociative feature

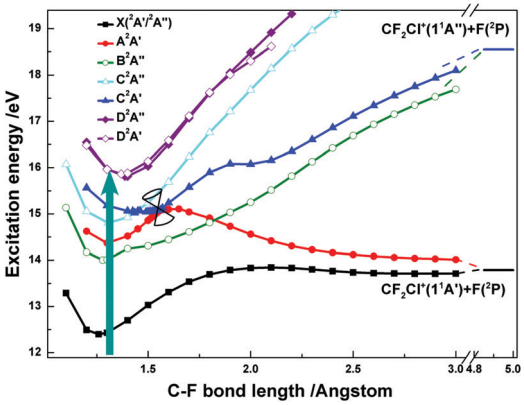

Fig. 6 F-loss potential energy curves of the low-lying electronic states of CF_3Cl^+ calculated at the TD-B3LYP/6-311+G(d) level, where the dark cyan arrow indicates the Franck–Condon region during photoionization.

along the C–F bond. A barrier with a height of 0.7 eV is found at *ca.* 1.56 Å owing to the avoiding of crossing by the upper C^2A' state. Moreover, when the C–Cl distance increases accompanied by Cl-loss, the barrier height slightly decreases to a lower value than the minimum of the C^2E state. Thus, the C–Cl and C–F bond cleavages of the A^2A' state could occur simultaneously when the excitation energy is beyond the barrier. At a lower energy, the Cl-loss channel should be much faster than the C–F bond rupture owing to its repulsive characteristics along the C–Cl bond.

Based on the calculated potential energy curves, it is impossible for CF_3Cl^+ in the $C(^2A'/^2A'')$ and $D(^2A'/^2A'')$ states to directly dissociate to produce the CF_2Cl^+ fragment. Thus, the CF_2Cl^+ fragment observed in the experiment must undergo a non-adiabatic process like internal conversion to the lower electronic states. We can exclude the bound X^2E state as the intermediate state, owing to the observed repulsive features (*e.g.* Gaussian-type total KRED) along the C–F bond cleavage. Thus, the A^2A' state is a unique candidate, and the electronic–vibrational coupling between C^2E (or D^2E) and A^2A' causes internal conversion prior to dissociation. The rate of the C–F bond cleavage in the A^2A' state should be somewhat slow according to the barrier, which is consistent with the observed results of branching ratios (Fig. 2).

3.5 F-loss mechanism of CF_3Cl^+ in C^2E and D^2E states

Combining the experimental and computational results, the F-loss mechanism of the CF_3Cl^+ cation in the C^2E and D^2E states can be proposed. For both the C^2E and D^2E ionic states, the unique C–F bond rupture mechanism must undergo an internal conversion to the lower A^2A' state, and then directly dissociate on the adiabatic potential energy surface of the latter. The similar F-loss mechanisms of CF_3Cl^+ in the C^2E and D^2E states in dissociative photoionization are summarized as follows.

$$CF_3Cl + h\nu \xrightarrow{\text{photoionization}} CF_3Cl^+(C^2E \text{ or } D^2E)$$

$$\xrightarrow{\text{internal conversion}} CF_3Cl^+\left(A^2A', v^+\right)$$

$$\xrightarrow{\text{direct dissociation}} CF_2Cl^+\left(X^1A'\right) + F\left(^2P\right)$$

As indicated in a previous study,[26] bimodal KERDs were observed in the Cl-loss process from CF_3Cl^+ in the C^2E and D^2E states, and only the parallel, fast dissociation component (shown by the lines in red color in Fig. 5) was produced based on the internal conversion to A^2A' followed by direct dissociation. Thus, only the fast dissociation components of the C–Cl cleavage should be compared with the total KERD of the C–F bond rupture. As shown in Fig. 5, the excess energy is populated on the kinetic energy of the fragments when the C–F bond is broken. The average total kinetic energy release along the C–F rupture at 16.99 and 17.85 eV are *ca.* 1.10 and 1.04 eV, respectively, while those along the C–Cl cleavage are only 0.56 and 0.60 eV. Moreover, the β values for the F-loss channel are 0.73 at 16.99 eV and 0.35 at 17.85 eV, and are larger than those of the Cl-loss pathway (0.34 at 16.99 eV and 0.15 at 17.85 eV). All these results indicate that for the CF_3Cl^+ cation in the C^2E and D^2E states, the C–Cl bond rupture occurs with a slower rate compared to that for the C–F bond cleavage.

The conclusion is very atypical, because there is a barrier along the C–F coordinate, and hence the F-loss usually occurs with a slower rate compared to the barrierless Cl-loss. However, for dissociation of the C^2E and D^2E states, the highly excited A^2A' state produced by internal conversion seems to favor the C–F rupture rather than the C–Cl cleavage. The atypical phenomenon strongly indicates that after internal conversion, the system crosses over to the A^2A' state past the barrier, where the F loss is impulsive and the repulsive force of F-loss is stronger than that of Cl-loss. In other words, the present observations provide new information on the A^2A' potential energy surface far from the Franck–Condon region. According to the C–F and C–Cl rupture mechanisms of CF_3Cl^+ in the C^2E and D^2E states, the internal conversion is the rate-determining step in the overall dissociative photoionization.

Moreover, owing to the similar kinetic energy distributions of the C^2E and D^2E states, the vibrational excitation of the intermediate A^2A' state after internal conversion should be almost the same in energy during the dissociative photoionization of CF_3Cl *via* the C^2E and D^2E ionic states, irrespective of the C–F and C–Cl bond ruptures. However, the internal conversion from D^2E to A^2A' is slower than the C^2E state, and thus molecular rotation occurs prior to dissociation leading to a smaller β value.

4. Conclusions

Combined with the VUV light from synchrotron radiation, the TPEPICO measurements were applied in the dissociative photoionization of CF_3Cl in the energy range of 12.30–18.50 eV. For the electronic excited states of the CF_3Cl^+ cation, both fragment ions, CF_3^+ and CF_2Cl^+, were observed in the coincident mass spectra. For the A^2A' and B^2A'' ionic states, the CF_3^+ ions dominated but the CF_2Cl^+ fragment ion appeared to have a very limited fraction. The branching ratio of the Cl-loss and F-loss channels showed a dependence on photon energy. The CF_2Cl^+ fragment was dominant in the dissociative photoionization *via* the C^2E and D^2E ionic states, and was kept constant. The adiabatic ionization energy (IE_a) of C^2E was determined from the inflection point to be approximately equal to 15.46 eV.

The 3D time-sliced images of the $CF_2{}^{35}Cl^+$ fragment were then recorded. From the acquired images, the total KERDs and angular distributions were derived. The total KERDs could be fitted very well with Gaussian functions, and the anisotropy parameters β were positive but smaller than two. All the results indicated that the C^2E and D^2E states exhibited a repulsive feature to some extent, but did not exhibit a direct dissociation along the repulsive potential energy surface. Furthermore, the larger β values for the F-loss channel compared to that for the C–Cl bond rupture suggested that the decomposition rate along the C–F bond is faster than that along the C–Cl coordinate.

To clarify the C–F bond cleavage mechanism from CF_3Cl^+ in electronically excited states, the F-loss potential energy curves were calculated based on the TD-B3LYP level. A predissociative barrier was located along the C–F bond rupture on the potential energy surface of the A^2A' state, owing to the interaction of the C^2A' state. Moreover, both the C^2E (C^2A' and C^2A'') and D^2E (D^2A' and D^2A'') states are bound along the C–F bond. Thus, the unique and reasonable F-loss mechanism applicable to the states is similar to the C–Cl bond rupture: internal conversion to the A^2A' state through strong electronic–vibration coupling and direct dissociation were achieved by crossing the barrier.

Based on the above experimental and theoretical conclusions, a full description of the F-loss mechanism from CF_3Cl^+ in the C^2E and D^2E states is proposed. Irrespective of whether the C–F and C–Cl bond ruptures, the internal conversion was the rate-determining step in the dissociative photoionization of CF_3Cl *via* the C^2E and D^2E ionic states. The observed faster C–F bond rupture is thought to shed light on new information on the A^2A' potential energy surface far from the Franck–Condon region. Moreover, to our surprise, the intermediate vibrational excited A^2A' state after the internal conversion looks almost the same in terms of the energy required for the C–F cleavage of CF_3Cl^+ in the C^2E and D^2E states, according to their identical kinetic energy distributions.

Conflicts of interest

There are no conflicts to declare.

Acknowledgements

The work was financially supported by the National Key Research and Development program of China (No. 2016YFF0200502), the National Natural Science Foundation of China (No. 21573210 and 21873089) and the National Key Basic Research Foundation of China (No. 2013CB834602). X. Zhou also thanks the USTC-NSRL Association for support funding.

References

1 A. C. Adams and C. D. Capio, *J. Electrochem. Soc.*, 1981, **128**, 366–370.
2 J. W. Coburn, *Plasma etching and reactive ion etching*, American Institute of Physics, New York, 1982.

3 J. R. Roth, *Industrial plasma engineering Vol. 1, Principles*, Institute of Physics Publishing, Bristol, *Filadelfia*, 1995.
4 F. S. Rowland and M. J. Molina, *Rev. Geophys.*, 1975, **13**, 1–35.
5 N. Washida, T. Imamura and H. Bandow, *Bull. Chem. Soc. Jpn.*, 1996, **69**, 535–541.
6 J. Doucet, P. Sauvageau and C. Sandorfy, *J. Chem. Phys.*, 1973, **58**, 3708–3716.
7 T. Cvitaš, H. Güsten and L. Klasinc, *J. Chem. Phys.*, 1977, **67**, 2687–2691.
8 R. Jadrny, L. Karlsson, L. Mattsson and K. Siegbahn, *Phys. Scr.*, 1977, **16**, 235–241.
9 R. Gilbert, P. Sauvageau and C. Sandorfy, *J. Chem. Phys.*, 1974, **60**, 4820–4824.
10 H. W. Jochims, W. Lohr and H. Baumgärtel, *Ber. Bunsen-Ges. Phys. Chem.*, 1976, **80**, 130–138.
11 W. Z. Zhang, G. Cooper, T. Ibuki and C. E. Brion, *Chem. Phys.*, 1991, **151**, 343–356.
12 J. W. Au, G. R. Burton and C. Brion, *Chem. Phys.*, 1997, **221**, 151–168.
13 M. Hoshino, K. Sunohara, C. Makochekanwa, L. Pichl, H. Cho and H. Tanaka, *J. Chem. Phys.*, 2007, **126**, 024303.
14 C. Brion, W. Stewart, D. Yee and P. Crowley, *J. Electron Spectrosc. Relat. Phenom.*, 1981, **23**, 399–415.
15 J. Creasey, I. Lambert, R. Tuckett and A. Hopkirk, *Mol. Phys.*, 1990, **71**, 1367–1380.
16 L. Lee, J. Han, C. Ye and M. Suto, *J. Chem. Phys.*, 1990, **92**, 133–139.
17 H. Biehl, K. Boyle, R. Tuckett, H. Baumgärtel and H. Jochims, *Chem. Phys.*, 1997, **214**, 367–381.
18 S. Cradock, E. A. V. Ebsworth and R. A. Whiteford, *J. Chem. Soc., Dalton Trans.*, 1973, 2401–2404.
19 Y. Uehara, N. Saito and T. Yonezawa, *Chem. Lett.*, 1973, 495–500.
20 W. Kischlat and H. Morgner, *J. Electron Spectrosc. Relat. Phenom.*, 1985, **35**, 273–288.
21 I. Novak, J. M. Benson and A. W. Potts, *J. Electron Spectrosc. Relat. Phenom.*, 1986, **41**, 175–179.
22 G. M. Bancroft, J. D. Bozek, J. N. Cutler and K. H. Tan, *J. Electron Spectrosc. Relat. Phenom.*, 1988, **47**, 187–196.
23 J. D. Bozek, G. M. Bancro, J. N. Cutler, K. H. Tan, B. W. Yates and J. S. Tse, *Chem. Phys.*, 1989, **132**, 257–270.
24 G. Cooper, W. Z. Zhang, C. E. Brion and K. H. Tan, *Chem. Phys.*, 1990, **145**, 117–129.
25 J. C. Creasey, D. M. Smith, R. P. Tuckett, K. R. Yoxall, K. Codling and P. A. Hatherly, *J. Phys. Chem.*, 1996, **100**, 4350–4360.
26 X. K. Wu, G. Q. Tang, H. H. Zhang, X. G. Zhou, S. L. Liu, F. Y. Liu, L. S. Sheng and B. Yan, *Phys. Chem. Chem. Phys.*, 2018, **20**, 4917–4925.
27 V. H. Dibeler, R. M. Reese and F. L. Mohler, *J. Res. Natl. Bur. Stand.*, 1956, **57**, 113–118.
28 C. J. Noutary, *J. Res. Natl. Bur. Stand., Sect. A*, 1968, **72**, 479–485.
29 J. M. Ajello, W. T. Huntress Jr and P. Rayermann, *J. Chem. Phys.*, 1976, **64**, 4746–4754.
30 I. Powis and C. J. Danby, *Chem. Phys. Lett.*, 1979, **65**, 390–394.
31 I. Powis, *Mol. Phys.*, 1979, **39**, 311–327.
32 X. F. Tang, X. G. Zhou, M. L. Niu, S. L. Liu, J. D. Sun, X. B. Shan, F. Y. Liu and L. S. Sheng, *Rev. Sci. Instrum.*, 2009, **80**, 113101.
33 A. Bodi, P. Hemberger, T. Gerber and B. Sztáray, *Rev. Sci. Instrum.*, 2012, **83**, 083105.
34 G. A. Garcia, B. K. Cunha de Miranda, M. Tia, S. Daly and L. Nahon, *Rev. Sci. Instrum.*, 2013, **84**, 053112.
35 X. F. Tang, M. L. Niu, X. G. Zhou, S. L. Liu, F. Y. Liu, X. B. Shan and L. S. Sheng, *J. Chem. Phys.*, 2011, **134**, 054312.
36 X. F. Tang, X. G. Zhou, M. L. Niu, S. L. Liu and L. S. Sheng, *J. Phys. Chem. A*, 2011, **115**, 6339–6346.
37 X. F. Tang, X. G. Zhou, M. M. Wu, Z. Gao, S. L. Liu, F. Y. Liu, X. B. Shan and L. S. Sheng, *J. Chem. Phys.*, 2013, **138**, 094306.
38 X. K. Wu, Z. Gao, T. P. Yu, X. G. Zhou and S. L. Liu, *Acta Phys.-Chim. Sin.*, 2017, **33**, 2004–2012.
39 X. F. Tang, X. G. Zhou, M. M. Wu, S. L. Liu, F. Y. Liu, X. B. Shan and L. S. Sheng, *J. Chem. Phys.*, 2012, **136**, 034304.
40 S. Wang, R. Kong, X. Shan, Y. Zhang, L. Sheng, Z. Wang, L. Hao and S. Zhou, *J. Synchrotron Radiat.*, 2006, **13**, 415–420.
41 H. Offerhaus, C. Nicole, F. Lepine, C. Bordas, F. Rosca-Pruna and M. Vrakking, *Rev. Sci. Instrum.*, 2001, **72**, 3245–3248.
42 B. Sztáray and T. Baer, *Rev. Sci. Instrum.*, 2003, **74**, 3763–3768.
43 A. Bodi, B. Sztáray, T. Baer, M. Johnson and T. Gerber, *Rev. Sci. Instrum.*, 2007, **78**, 084102.
44 M. J. Frisch, G. W. Trucks, H. B. Schlegel, G. E. Scuseria, M. A. Robb, J. R. Cheeseman, G. Scalmani, V. Barone, B. Mennucci, G. A. Petersson and H. Nakatsuji, *Gaussian 09 D.01*, Gaussian, Inc., Wallingford CT, 2009.
45 K. E. Holdy, L. C. Klotz and K. R. Wilson, *J. Chem. Phys.*, 1970, **52**, 4588–4599.
46 R. N. Zare, *Mol. Photochem.*, 1972, **4**, 1–37.
47 P. Hemberger, A. Bodi, T. Gerber, M. Würtemberger and U. Radius, *Chem. – Eur. J.*, 2013, **19**, 7090–7099.
48 X. K. Wu, M. M. Wu, X. F. Tang, X. G. Zhou, S. L. Liu, F. Y. Liu and L. S. Sheng, *J. Phys. Chem. A*, 2017, **121**, 4743–4753.